



Mechanism of intra- and inter-molecular C=C bond formation of propanal on Brønsted acid sites contained within MFI zeolites



Fan Lin, Ya-Huei (Cathy) Chin *

Department of Chemical Engineering and Applied Chemistry, University of Toronto, Toronto, Canada

ARTICLE INFO

Article history:

Received 24 July 2013

Revised 7 November 2013

Accepted 19 November 2013

Keywords:

Alkanal

Deoxygenation

MFI zeolite

Brønsted acid

Inter-molecular C=C bond formation

Intra-molecular C=C bond formation

Aldol condensation

Hydrogen transfer

Olefin

Propanal

ABSTRACT

Kinetic and chemical titration studies are used to unravel the reaction pathways and catalytic requirements for propanal deoxygenation over Brønsted acid sites contained within MFI zeolites. Propanal deoxygenation in the absence of external hydrogen source is initiated via primary and competitive pathways of inter- and intra-molecular C=C bond formation that involve bimolecular coupling of propanal and unimolecular deoxygenation steps, respectively. The inter-molecular C=C bond formation proceeds via mechanistic steps resembled the acid-catalyzed aldol condensation reactions in the homogeneous phase, and its reactive collision frequencies increase with increasing propanal pressure. The reaction is initiated by keto–enol tautomerization of propanal to form small concentrations of propenol. The propenol undergoes kinetically-relevant nucleophilic attack to protonated propanal, the most abundant surface intermediates, to create the inter-molecular C=C bond. The competitive uni-molecular deoxygenation step involves kinetically-relevant hydrogen transfer from hydrogen-donating agents and occurs at rates that remain invariance with propanal pressure. Hydrogen-donating agents are aliphatic rings produced from consecutive inter-molecular C=C bond formation and ring closure events and donate hydrogen via dehydrogenation steps to increase their extent of unsaturation. Hydrogen-donating events must kinetically couple with the direct hydrogen insertion step on propanal to satisfy the deoxygenation stoichiometry and form propanol, which upon dehydration evolves predominantly propene, thus preserving the carbon backbone. Water as a by-product prevents binding of larger, inactive carbonaceous species on acid sites and inhibits the inter-molecular C=C bond formation step by increasing the reverse rate of this step. Water, however, does not alter the net rate for intra-molecular C=C bond formation, because of its irreversible nature. An increase in the rate ratio for intra- over inter-molecular C=C bond formation upon the addition of 3-methyl-1-pentene, an effective hydrogen-donating agent, confirms the kinetic relevance of the hydrogen transfer step for propene formation. These findings on the different kinetic dependencies for the competitive reactions and their mechanistic interpretations provide the operating strategies to tune the reaction pathways, manipulate the extent of hydrogen transfer, and tailor the distributions of larger oxygenates and alkenes during propanal deoxygenation reactions.

© 2013 Elsevier Inc. All rights reserved.

1. Introduction

Small oxygenates of alkanal and alkanone (R–CHO, RC(=O)R'; R ≤ 4) produced from biomass pyrolysis could be catalytically upgraded to value-added chemicals, hydrocarbons, or aromatics [1–3] by reactions that remove oxygen heteroatoms and lengthen their carbon backbone. The aldol-type condensation reactions couple alkanal (R–CHO) or alkanone (RC(=O)R') reactants to increase their carbon chain length and eject an oxygen atom as H₂O without the use of external H₂ [2,4,5]. The condensation reactions may occur in acidic and basic medium and, in the homogenous phase, mechanistic pathways and catalytic functions of acid and base

have been well established [6]. The acid-catalyzed C–C bond formation [6–8] occurs via an initial keto–enol tautomerization of alkanal (or alkanone) to form the conjugate enol. The sequential nucleophilic attack of the alpha carbon in enol to the protonated carbonyl group of alkanal (or alkanone) creates an inter-molecular C–C bond, thus lengthening the carbon backbone and forming a beta-hydroxy alkanal (or alkanone), also known as an aldol. The base-catalyzed C–C bond formation [6] involves the formation of a resonance-stabilized enolate and its sequential nucleophilic attack to the carbonyl group of an alkanal or alkanone to evolve the aldol. Both acid- and base-catalyzed reactions share a common sequential dehydration step that transforms the beta-hydroxyl alkanal (or alkanone) to an alkenal or alkenone, respectively, to complete a catalytic turnover [6].

* Corresponding author. Fax: +1 (416) 978 8605.

E-mail address: cathy.chin@utoronto.ca (Ya-Huei (Cathy) Chin).

Similar reactions have been reported on acid sites [9–11], basic sites [12,13], or bifunctional acid–basic site pairs [14–17] immobilized within solid structures. Condensation reactions on solid basic sites (e.g., on Mg–Al mixed oxide) form almost exclusively the expected primary condensation products at low temperatures (353–413 K) [12,13]. Mg–Al mixed oxides catalyze heptanal and benzaldehyde reactions to form a mixture of cross-condensation (jasminaldehyde) and self-condensation (2-*n*-pentyl-2-nonenal) products at selectivities of 67–80% and 20–33%, respectively, at 403 K [12,13]. Alkali ion-exchanged zeolites (Na–X, K–X, and Cs–X), alkali-treated alumina (KOH–Al₂O₃), and hydrotalcite {[Mg_{0.6}Al_{0.4}(OH)₂](CO₃)_{0.20}·0.84H₂O} convert propanal to 2-methyl-2-pentenal and 3-hydroxyl-2-methylpentanal (373 K) [12]. Similarly, alkaline earth metal oxides (e.g., MgO and SrO) promote butanal condensation to form predominantly the self-condensation product (2-ethyl-2-hexenal) at carbon selectivities above 90% with a small amount of 2-ethyl-2-hexenol, heptanone, and 2-ethylhexanol at 573 K [14]. As the temperature increases, ketonization, reverse α -addition, cracking, and decarboxylation reactions begin to occur on basic sites (e.g., on MgO/SiO₂ [14], SrO/SiO₂ [14], and Ce_xZr_{1-x}O₂ [18]) at detectable rates relative to those of primary condensation reactions, as reported for propanal reactions on MgO/SiO₂ and SrO/SiO₂ (>723 K) [14] and butanal reactions on Ce_xZr_{1-x}O₂ (>673 K) [18].

On Brønsted acid catalysts (H-MFI) [4,5,19], the initial coupling of alkanals leads to larger oxygenates, which undergo secondary reactions of aromatization, alkylation/dealkylation, and cracking. At higher temperatures (e.g., 673 K), these secondary reactions occur much faster than the initial alkanal turnovers and lead to diverse methyl- or ethyl-substituted aromatics (e.g., trimethylbenzene, methyl-ethylbenzene) and light gases (e.g., CO, CO₂, C₁–C₃ hydrocarbons). The primary condensation products were detected on H-MFI at these higher temperatures only when introducing alkanal reactant in pulses to maintain the pressures of alkanal and primary products at low values [4].

Condensation, aromatization, and cracking reactions during alkanal conversions on Brønsted acid sites (H⁺) contained within microporous crystalline silica–alumina frameworks have been recently proposed to involve pools of oxygenate and hydrocarbon intermediates coexisting within the zeolitic pores [4]. The primary and secondary nature of these reactions, rate dependencies of individual catalytic paths, identity of kinetically-relevant steps, and associated mechanistic details have not been rigorously established. The lack of such molecular level details is caused, in large part, by the complexity of the reaction network. The mechanistic knowledge, kinetic dependencies, and site requirements for the C–C bond formation and oxygen removal are, however, crucial for predicting and tailoring the product distributions and their yields.

Herein, we interrogate the fate of propanal during their catalytic sojourns over Brønsted acid sites (H⁺) contained within MFI framework. We propose a sequence of elementary reactions to describe the fate of propanal in competitive reactions that create an inter- and intra-molecular C=C bond to evolve 2-methyl-2-pentenal and propene, respectively. We also discuss secondary reactions of ring closure, dehydration, and dehydrogenation that evolve the larger aromatics and requirements of hydrogen transfer between the secondary dehydrogenation step and the intra-molecular C=C bond formation step to satisfy the reaction stoichiometry. We draw a mechanistic synergy between the reactions occurring at acid sites contained within the microporous crystalline materials and those in the homogeneous phase and then report a competitive direct deoxygenation path undetected in homogeneous reactions. The rate dependencies for these reactions were measured, their kinetic relevance and reversibility were interrogated, and the kinetic couplings of hydrogen transfer within the catalytic sequence were confirmed.

2. Experimental

2.1. Catalyst synthesis

MFI zeolite samples in their NH₄⁺ form (425 m² g⁻¹, Si/Al atomic ratio = 11.5, CBV2314, Zeolyst) were treated in flowing dry air (0.6 cm³ g⁻¹ s⁻¹, zero grade, Linde) to 873 K by increasing the temperature at 0.0167 K s⁻¹ and holding for 4 h to convert NH₄⁺ to H⁺. In a separate series of MFI zeolite samples, ion exchange was performed to exchange the NH₄⁺ ions with Na⁺ ions to attain final samples with varying H⁺ and Na⁺ contents (atomic ratios of H⁺/Al = 0.82–0.48 and Na⁺/Al = 0–0.34). NH₄⁺-MFI zeolites (Si/Al = 11.5, 4 g) were mixed and stirred with aqueous NaCl solution {7.8–70 g of NaCl (99%, ACP Chemicals) and 100 cm³ of doubly deionized water} at 298 K for 24 h. The samples were then washed in doubly deionized water and filtered under vacuum until Cl⁻ ions in the filtrate were undetected from chemical titration with 0.1 mol L⁻¹ AgNO₃ (99.9999%, Sigma Aldrich) aqueous solution. The samples were dried at 393 K for at least 8 h and then heated in flowing dry air (0.6 cm³ g⁻¹ s⁻¹, zero grade, Linde) at 0.0167 K s⁻¹ to 873 K and holding for 4 h at 873 K to convert NH₄⁺ to H⁺.

2.2. Catalytic rates and selectivities of propanal and 1-propanol reactions on MFI zeolites

Chemical turnover rates and selectivities of propanal reactions were measured in a fixed bed tubular microcatalytic quartz reactor (inner diameter of 9.5 mm) with plug-flow hydrodynamics and operated under continuous flow mode. The reactor was contained within a resistively heated furnace with its temperature regulated using a digital feedback temperature controller. Catalyst samples (300 mg) were supported on a quartz frit and the reaction temperature was recorded using a K-type thermocouple placed at the center of the axial and radial directions of the catalyst bed.

Catalysts were heated in flowing He (2.8 cm³ g⁻¹ s⁻¹, Grade 5.0, Linde) at 0.0167 K s⁻¹ to reaction temperatures (473–673 K) prior to rate measurements. Propanal (Kosher grade, $\geq 97\%$, Sigma Aldrich) was used as received and introduced via a gas tight syringe (Model 008025, 1 cm³, SGE) mounted on a syringe infusion pump (Model LEGATO 100, KD Scientific) into a vaporizing zone, in which it was evaporated and mixed with a He purge stream (0.83 cm³ s⁻¹, Grade 5.0, Linde) at 320 K. All gas lines for transferring reactant mixtures were heated to 320 K and product mixtures were heated to 473 K to prevent condensation. Reactions of 1-propanol ($\geq 99.9\%$, Sigma Aldrich) on H-MFI were carried out following the same procedure with 0.58 kPa 1-propanol and at a space velocity of 6×10^{-4} mol 1-propanol (mol H₁⁺ s)⁻¹.

Reactions using propanal and water (C₃H₆O–H₂O) or propanal and 3-methyl-1-pentene (C₃H₆O–C₆H₁₂) feed mixtures were carried out by introducing either doubly deionized H₂O or 3-methyl-1-pentene (99%, Sigma Aldrich) into a second vaporizing zone maintained at 363 K or 330 K, respectively, located downstream from the vaporizer used for propanal evaporation (described above). Doubly deionized H₂O or 3-methyl-1-pentene was introduced via a gas tight syringe {Model 1005, 5 cm³ (Hamilton) for H₂O and Model 006230, 0.25 cm³ (SGE) for C₆H₁₂ infusion} mounted on a syringe infusion pump (Model KDS-100, KD Scientific, for H₂O or Model LEGATO 100, KD Scientific, for C₆H₁₂ infusion).

Chemical species in the feed and reactor effluent stream were quantified using an online gas chromatograph (Model 7890A, Agilent) and mass spectrometer (Model 5975C, Agilent), GC–MS, equipped with a 10-port sampling valve containing two sample loops of 250 μ L each. The samples contained in the gas sampling

loops were analyzed by chromatographic separation using two capillary columns (HP-5MS, Agilent, 190091S-433, 30 m, 0.25 mm ID and HP-5, Agilent, 19091J-413, 30 m, 0.32 mm ID). The HP-5 column is connected to thermal conductivity (TCD) and flame ionization (FID) detectors in series and the HP-5MS column to the MS detector.

2.3. Chemical titration of Brønsted acid sites

The number of Brønsted acid sites present initially (denoted by H_i^+ ; herein and after, subscript “i” represents the initial H^+ site density) and remained after reactions (denoted by H_r^+ , refer to working H^+ sites without binding to larger, inactive carbonaceous species) was determined from pyridine titration at 473 K on samples treated in flowing dry air (Section 2.1) or after rate measurements (Section 2.2), respectively. Acid site titrations on air-treated MFI samples were carried out on 300 mg samples after *in situ* heat treatment to 473 K at a constant heating rate of 0.0167 K s^{-1} under flowing He ($0.83 \text{ cm}^3 \text{ s}^{-1}$). Acid site titrations on samples after propanal reactions were carried out upon the removal of propanal feed and purging under flowing He ($0.83 \text{ cm}^3 \text{ s}^{-1}$) at 473 K for 1800 s. After these respective treatments, pyridine was introduced at $3.42 \times 10^{-8} \text{ mol s}^{-1}$ via a gas tight syringe (Model 006230, 0.25 cm^3 , SGE) into a vaporization zone maintained at 391 K, in which it was evaporated and mixed with a flowing He stream. The pyridine/He mixture was then introduced to the sample and the amount of pyridine in the effluent stream was quantified using the flame ionization (FID) detector on the gas chromatograph (Model 7890A, Agilent). The titration was completed when the molar flow rate of pyridine in the effluent stream became identical to that of the feed stream. The number of H^+ site was determined based on the pyridine uptakes assuming a pyridine-to- H^+ molar ratio of unity. The relative amount of Brønsted and Lewis acid sites was also determined from integrated intensities of pyridine adsorption bands from infra-red spectrum of pyridine adsorption on the H-MFI samples at 1540 cm^{-1} and 1450 cm^{-1} , respectively, at 423 K.

2.4. Temperature programmed desorption of surface intermediates after propanal reactions on MFI zeolites

Temperature programmed desorption (TPD) was performed on the catalyst (300 mg MFI zeolite) after propanal reactions ($1.1 \text{ kPa C}_3\text{H}_6\text{O}$, $1.1 \times 10^{-3} \text{ mol C}_3\text{H}_6\text{O} (\text{mol H}_i^+ \text{ s}^{-1})$) for 960 s at 473 K in the microcatalytic quartz reactor described in Section 2.2, followed by purging under flowing He ($0.83 \text{ cm}^3 \text{ s}^{-1}$) for 1800 s at 473 K to remove residual propanal from the transfer lines. The sample was heated under flowing He ($0.83 \text{ cm}^3 \text{ s}^{-1}$) at a constant heating rate of 0.0167 K s^{-1} to increase the catalyst bed temperature from 473 to 673 K linearly and held isothermally at 673 K for 1800 s. The composition of the effluent stream was analyzed using the GC–MS (described in Section 2.2).

3. Results and discussion

3.1. Reaction network and product distributions during catalytic deoxygenation of propanal on H-MFI zeolites

Figs. 1 and 2 show turnover rates and product distributions, respectively, for propanal reactions on H-MFI zeolites (Si/Al = 11.5) between 473 and 673 K and Appendix A.1 summarizes the associated carbon balances. At 473 K, propanal reactions formed light alkenes (predominantly propene), larger oxygenates (predominantly 2-methyl-2-pentenal and 2,3,4,5-tetramethyl-2-cyclopentenal), aromatics (predominantly trimethylbenzenes and

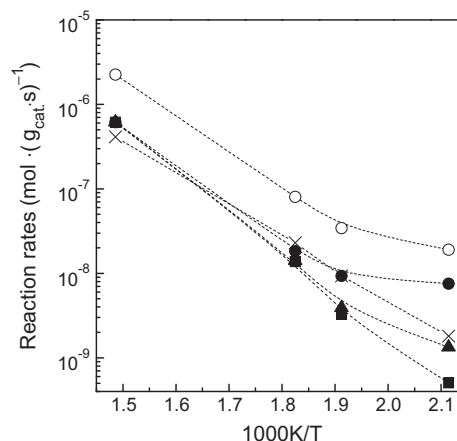


Fig. 1. Temperature dependence of propanal conversion rates (\circ) and the rates of olefin (C_3-C_6 , \times), $C_6H_{10}O$ (2-methyl-2-pentenal, \bullet), $C_9H_{14}O$ (2,3,4,5-tetramethyl-2-cyclopentenal and isomers, \blacktriangle), aromatic (C_6-C_{12} , \blacksquare) formation during propanal (C_3H_6O) reactions on H-MFI zeolites (Si/Al = 11.5, 7.5 ks, $1.1 \times 10^{-3} \text{ mol C}_3\text{H}_6\text{O} (\text{mol H}_i^+ \text{ s}^{-1})$ (subscript i denotes the initial acid site density), 1.1 kPa C_3H_6O in He).

dimethylbenzenes), and a small amount of CO and CO_2 ($\{(r_{CO} + r_{CO_2})/r_{overall}\} < 0.01$, 473 K, where r_{CO_2} , r_{CO} , $r_{overall}$ denote the CO_2 and CO formation rates and the overall propanal conversion rate, respectively). As the reaction temperature increased from 473 to 548 K, the carbon fractions of aromatic and olefinic species in the reactor effluent stream increased from 13.1% to 51.4% and from 9.5% to 33.4%, respectively, while the carbon fraction of oxygenates concomitantly decreased from 65.2% to 10.2% (Fig. 2a–c). At 673 K, oxygenates were undetected, because of their rapid conversion to aromatic and olefinic species, which became the predominant products with carbon distributions of 81.6% and 18.3%, respectively (Fig. 2d). Within the olefinic and aromatic fractions, the species diversity increased with increasing temperature, and the predominant species were propene, toluene, xylene, methyl-naphthalene, and dimethylnaphthalene as the temperature reached 673 K, as shown in Fig. 2d.

Propanal conversion rates increased with temperature to values much larger than expected from extrapolation of the rate data at lower temperatures (473–548 K, Fig. 1) using the Arrhenius relation. Rates at 673 K exceeded the expected values by at least two orders of magnitude. These temperature effects on rates indicate that additional reaction pathways, apparently those with higher effective activation energies, become the predominant propanal conversion routes at higher temperatures. The higher temperatures and prevalent higher pressures of aromatics (mono-, di-, and tri-methylbenzenes) and alkenes (ethylene, propylene, and butene) promote additional reaction pathways, which may include the hydrocarbon pool typed mechanism, as established previously for methanol-to-olefin or methanol-to-gasoline synthesis on MFI zeolites [20–23].

Scheme 1 shows a proposed reaction network for propanal reactions on Brønsted acid sites. This reaction network captures the competitive bimolecular and uni-molecular reaction pathways that create the inter- and intra-molecular C=C bond to evolve 2-methyl-2-pentenal ($C_6H_{10}O$) and propene (C_3H_6), respectively, and the sequential ring closure and alkylation–dealkylation reactions that form larger aromatics and oxygenates (>6 carbon atoms). Bimolecular reactions of propanal create inter-molecular C–C bond before H_2O elimination to form 2-methyl-2-pentenal as the primary product (R 1.1, Scheme 1). The 2-methyl-2-pentenal undergoes sequential coupling with propenol (from propanal tautomerization step, R 2.1) and H_2O elimination (R 1.2) to evolve 2,4-dimethyl-2,4-heptadienal ($C_9H_{14}O$). The 2,4-dimethyl-2,4-

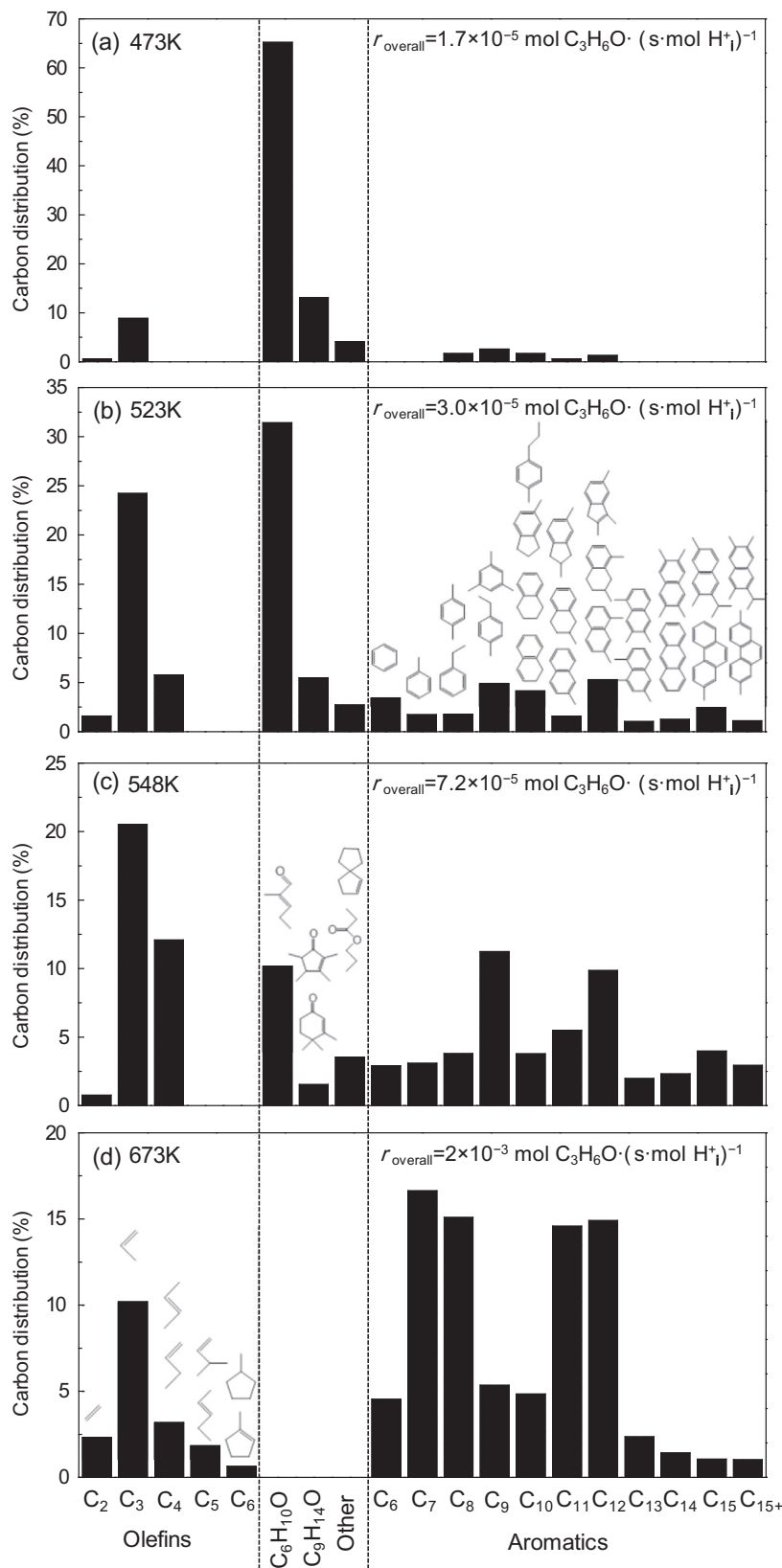
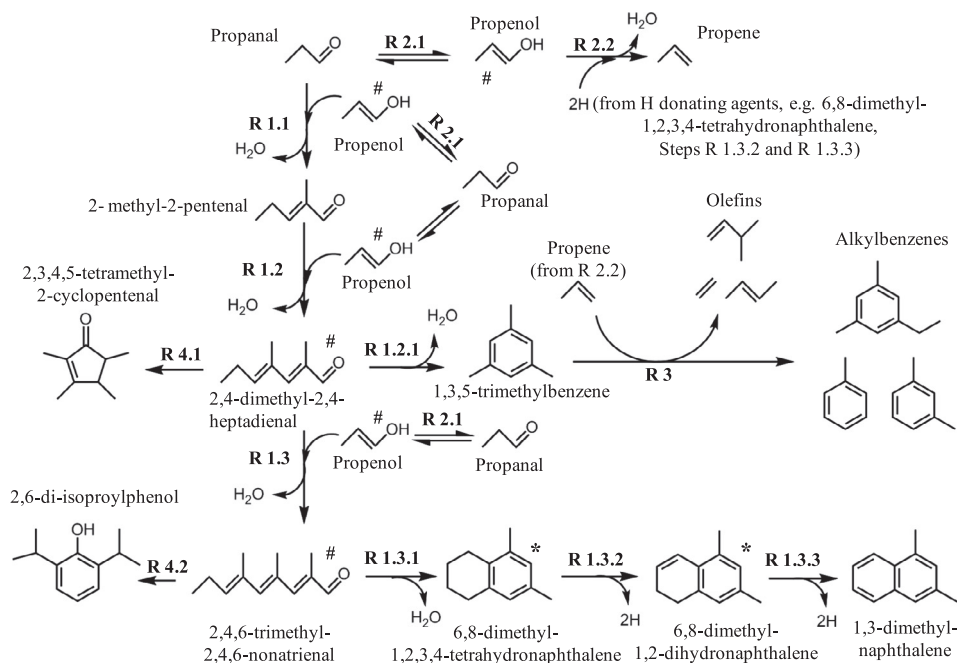


Fig. 2. (a–d) Carbon distributions in the product of propanal (C_3H_6O) reactions on H-MFI zeolite (Si/Al = 11.5) at 473 K (a), 523 K (b), 548 K (c), and 673 K (d) (7.5 ks, 1.1×10^{-3} mol C_3H_6O (mol H^+ s) $^{-1}$, 1.1 kPa C_3H_6O in He, $r_{overall}$ is the overall C_3H_6O conversion rate; chemical structures of the most abundant species are shown and isomers of these species were also detected).

heptadienal may undergo a ring closure step followed by isomerization (R 4.1) to form predominantly 2,3,4,5-tetramethyl-2-cyclopentenol and a small amount of oxygenated isomers or,

alternatively, a ring closure and H_2O elimination step (R 1.2.1) to create an intra-molecular C=C bond and evolve 1,3,5-trimethylbenzene (C_9H_{12}). Sequential alkylation and dealkylation of



Scheme 1. Reaction network for propanal turnover on H-MFI zeolite (#: Intermediates at undetectable concentrations; *: Hydrogen-donating agents for deoxygenation reaction in R 2.2).

trimethylbenzene (R 3) lead to diverse aromatic species containing 6–12 carbon atoms (carbon distributions shown in Fig. 2). In parallel to the bimolecular reaction (R 1.1), propanal may undergo deoxygenation to remove the oxygen heteroatom by its recombination with two external H atoms to eject H₂O, forming an intra-molecular C=C bond to evolve propene (R 2.1 and R 2.2). At higher temperatures, secondary reactions of dehydrogenation, hydrogen transfer, and alkylation–dealkylation steps that shuffle methyl groups and hydrogen atoms become much faster than the initial inter- and intra-molecular C=C bond formation in propanal (R 1.1 and R 2.1–2.2) and secondary condensation reactions (R 1.2–1.3). These secondary reactions lead to diverse olefinic and aromatic products with carbon distributions shown in Fig. 2. In the next sections, we provide the mechanistic evidences on the primary and secondary nature of the reaction steps proposed in Scheme 1. We first probe and then confirm the accessibility of all Brønsted acid sites that are contained within the MFI framework to propanal reactants in Section 3.2 and then interrogate the specific catalytic requirements and kinetic dependencies for the competitive bimolecular (R 1.1) and uni-molecular (R 2.2) reactions that create the inter- and intra-molecular C=C bond within propanal to evolve 2-methyl-2-pentalen and propene, respectively, in Sections 3.3 and 3.4. The reversibility of the kinetically-relevant steps and the kinetic relevance of hydrogen transfer are discussed in Sections 3.5 and 3.6.

3.2. Accessibilities of Brønsted acid site to propanal reactant and effects of acid site density on propanal conversion rates

Infra-red spectroscopic studies of pyridine adsorption on the H-MFI (Si/Al = 11.5) samples used in this study shows pyridine adsorption on Brønsted acid sites at 1540 cm⁻¹ and Lewis acid sites at 1450 cm⁻¹. The integrated intensities of these peaks, after correction with their respective extinction coefficients, show that 86.7% of the total sites are Brønsted acid sites while the rest are Lewis acid sites. H₂O by-products from inter- and intra-molecular C=C bond formation reactions either rehydrate the unsaturated aluminum sites (Lewis sites) on non-framework alumina to form

surface hydroxyl species or physisorb on these sites [9,24], thus preventing them from participation in catalysis. Thus, steady-state propanal conversion rates (>7.5 ks) reflect predominantly the contributions from Brønsted acid sites, their amount available for propanal catalysis was quantified by pyridine titration after exposure the catalysts to reaction mixtures.

The vast majority of Brønsted acid sites (H⁺) participated in catalytic turnovers are predominantly occupied by propanal (C₃H₆O) and its isomers during catalysis at 473 K and 1.1–4.5 kPa of C₃H₆O, a condition required for the rates of inter- and intra-molecular C=C bond formation to vary proportionally to and remain independent of propanal pressure, respectively, as shown later in Sections 3.3 and 3.4. The requirements of propanal and its isomers as the most abundant surface intermediates are independently confirmed next from temperature programmed desorption carried out on H-MFI (Si/Al = 11.5) after propanal catalysis at 473 K {1.1 kPa C₃H₆O, 960 s, 1.23 × 10⁻⁶ mol C₃H₆O (g_{cat.} s)⁻¹}.

Fig. 3 shows the temperature programmed desorption profile, plotted as the rate of desorption of carbonaceous species (per H⁺ site) from the H-MFI sample vs. temperature. Aromatics (94% C₈–C₁₂) and a small amount of light alkenes (6% C_nH_{2n}, n = 2–3) are the predominant species desorbed from the sample, because adsorbed intermediates would undergo inter-molecular C=C bond formation and ring closure steps (Pathways R 1.2–1.2.1 and R 1.2, 1.3, and 1.3.1, Scheme 1) before their desorption as larger aromatic species or cracking of these larger species to form the small amount of alkenes. Integration of the desorption rates in Fig. 3 over the entire temperature range gives the cumulative amount of carbon desorbed from the H-MFI catalyst. This amount, in term of carbon-to-H⁺ (C/H⁺) atomic ratio, was found to be 3.15. The value translates to a C₃H₆O-to-H⁺ molar ratio of near unity (1.05) during steady-state catalysis. This value, taken together with the first-order rate dependence for the inter-molecular C=C bond formation (Section 3.3) and zero-order dependence for the intra-molecular C=C bond formation (Section 3.4) in propanal, is consistent with binding of propanal or its isomers to H⁺ sites as the most abundant surface intermediates. The value infers that all H⁺ sites were accessible to propanal.

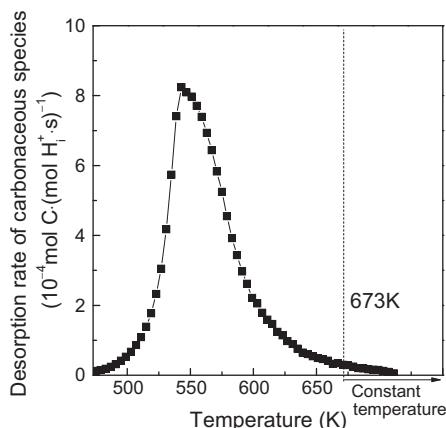


Fig. 3. Desorption rate of carbonaceous species from H-MFI catalyst as a function of temperature. The temperature programmed desorption was performed after exposure of the catalyst to propanal (C_3H_6O) reactions for 960 s at 473 K (300 mg H-MFI, Si/Al = 11.5, 0.0167 K s^{-1} , propanal reaction conditions: 1.1 kPa C_3H_6O in He, $1.23 \times 10^{-6} \text{ mol } C_3H_6O (\text{g}_{\text{cat.}} \text{ s})^{-1}$).

All of the H^+ sites in the 10-member ring MFI channels (diameter of $\sim 0.55 \text{ nm}$) are accessible to propanal, a compound with an estimated kinetic diameter of $0.45\text{--}0.50 \text{ nm}$ (based upon the kinetic diameters for alkane/alkene/alcohol with three or four carbon atoms [25,26]), because these sites are accessible to molecules with comparable (C3–C6 *n*-alkanes, $0.43\text{--}0.50 \text{ nm}$ [27]) and larger (pyridine, used here as the titrant, 0.59 nm [28]) kinetic diameter values. The accessibilities of all H^+ sites to propanal are also confirmed from rate measurements on a series of MFI zeolites (Si/Al = 11.5) with different H^+ -to- Na^+ ratios (molar ratios of H^+ /Al and Na^+ /Al are 0.82–0.48 and 0–0.34, respectively). The overall rates of propene formation (r_{intra}) from the primary deoxygenation route (R 2.1 and 2.2, Scheme 1) are plotted as a function of H^+ and Na^+ site densities in Fig. 4. The rates of propene formation (per mass of MFI sample) decreased proportionally with the decrease in H^+ site density and thus the increase in Na^+ site density, as these site densities were interrelated (the sum of H^+ and Na^+ site density equals 82% of the nominal Al density). Extrapolation of the propene formation rates to zero H^+ site density gave propene formation rates below detectable values because substitution of H^+ with Na^+ ions removed the Brønsted acid sites required for the direct deoxygenation reaction (R 2.2, Scheme 1). Rates for propene for-

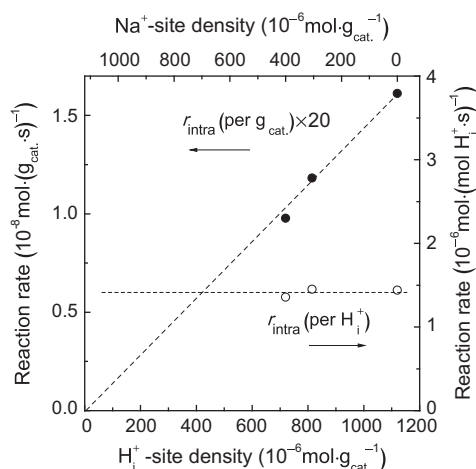


Fig. 4. Overall rates (per mass of catalyst, ●) and turnover rates (per H^+ , subscript i denotes the initial acid site density, ○) for intra-molecular C=C bond formation in propanal (C_3H_6O) on H-MFI plotted as a function of H^+ and Na^+ concentration (473 K, Si/Al = 11.5, 7.5 ks, $1.23 \times 10^{-6} \text{ mol } C_3H_6O (\text{g}_{\text{cat.}} \text{ s})^{-1}$, 1.1 kPa C_3H_6O in He).

mation (per mass of MFI sample, r_{intra} (per $\text{g}_{\text{cat.}}$)) are strictly proportional to H^+ site densities with an extrapolated rate value of zero for MFI samples without any H^+ site (Fig. 4). These rate values (per mass of MFI sample) led to constant turnover rates (per H^+ site) of $1.42 \times 10^{-6} \pm 0.03 \times 10^{-6} \text{ mol } (\text{mol } H^+ \text{ s})^{-1}$ (473 K) for propene formation, irrespective of the initial H^+ site density ($0.72 \times 10^{-3}\text{--}1.12 \times 10^{-3} \text{ mol } H^+ \text{ g}_{\text{cat.}}^{-1}$). Substitution of H^+ with Na^+ , however, increased the rates of bimolecular reaction (R 1.1, Scheme 1), because Na^+ sites catalyze propanal condensation much more effectively than H^+ sites via a separate, base-catalyzed aldol condensation pathway. Framework oxygen ions conjugated to Na^+ sites act as weak base [29] and abstract the α -hydrogen on propanal to form carbanion intermediates [30], which undergo nucleophilic addition to the carbonyl group of another propanal and, upon dehydration, create the inter-molecular C=C bond. The constant turnover rate values for propene formation irrespective of H^+ site density (Fig. 4), together with a C_3H_6O -to- H^+ surface molar ratio of 1.05 after catalysis (Fig. 3), led us to conclude that all H^+ sites within the MFI zeolites were accessible to propanal and these sites were kinetically equivalent (for propene turnovers). Next, we report kinetic dependencies and catalytic requirements for the inter- and intra-molecular C=C bond formation, interrogated under conditions that minimize both the secondary reactions (alkylation, cracking, etc.) and involvement of hydrocarbon pool mechanism. These conditions were attained by rate measurements under differential conditions (<5% propanal conversion), a high space velocity $\{1.1 \times 10^{-3} \text{ mol } C_3H_6O (\text{mol } H^+ \text{ s})^{-1}\}$, and at a moderate temperature (473 K).

3.3. Kinetic dependencies, elementary steps, and site requirements for inter-molecular C=C bond formation of propanal on H-MFI zeolites

Rates for bimolecular propanal reaction that creates an inter-molecular C=C bond and lengthens the carbon chain (R 1.1, Scheme 1) were measured at different propanal pressures (1.1–4.5 kPa) on H-MFI (Si/Al = 11.5) at 473 K. Turnover rates for this reaction, r_{inter} , were calculated based on the number of H^+ site available during reaction (determined from pyridine titration, Section 2.3), because condensation reactions of propanal produce heavy compounds (e.g., naphthalenes) which can gradually deposit on the catalysts and reduce the amount of H^+ sites available for catalytic turnovers, especially at the longer times (e.g., 7.5 ks for rate data reported herein). The rate values at 7.5 ks, which reflect the steady-state catalytic rates, are plotted as a function of C_3H_6O pressure in Fig. 5. Turnover rates for inter-molecular C=C bond formation (r_{inter}) increased linearly with C_3H_6O pressure ($P_{C_3H_6O} = 1.1\text{--}4.5 \text{ kPa}$), following the expression of:

$$r_{\text{inter}} = k_{\text{inter,eff}} P_{C_3H_6O} \quad (1)$$

where $k_{\text{inter,eff}}$ is the effective rate constant for inter-molecular C=C bond formation. We next propose a sequence of elementary steps, as presented in Scheme 2, from which we derive a rate expression that accurately describes the observed first-order rate dependence on C_3H_6O pressure.

Propanal (1) and propenol (2) interconvert rapidly within the intra-zeolitic channels (Step 2.1a, Scheme 2), thus these species are treated as a kinetically indistinguishable chemical lump and their relative pressures are dictated by the thermodynamics of keto–enol tautomerization reaction. Propanal may adsorb at the Brønsted acid sites (H^+) in diverse isomeric configurations of protonated propanal (3), propenol (4a), allyl alcohol (4b), or in the physisorbed forms of these species via single or multiple hydrogen bonds between the H^+ and the oxygen atom in these species and/or between the lattice oxygen and the hydrogen on propanal isomers. The adsorption configurations of similar carbonyl compounds (e.g.,

acetone) on acidic zeolites (MFI [31–35], Y [32]) have been probed using ^{13}C NMR studies. The formation of surface enol has been previously confirmed from H/D exchange between adsorbed acetone- d_6 and H^+ sites and between ^{13}C -2-acetone and D^+ sites in MFI zeolites at ambient temperature [31] and from the appearance of signal at ~ 180 ppm on ^{13}C NMR spectra as acetone adsorbed on H-MFI and H-Y between 298 and 453 K [32]. The formation of hydrogen bonded propanal from the less stable allyl alcohol¹ was confirmed from the feature at 216 ppm in ^{13}C NMR spectrum emerged during adsorption of allyl alcohol on H-MFI between 400 and 425 K [33]. Density functional theory (DFT) calculations on alcohol ($\text{C}_n\text{H}_{2n+1}\text{OH}$, $n = 1\text{--}4$) adsorption in H-MFI structures show a broad and shallow potential energy well between the protonated and hydrogen bonded species with small energy differences (between -1 and $+6$ kJ mol^{-1} for $\text{C}_n\text{H}_{2n+1}\text{OH}$, where $n = 1$ [36–38], 2 [38], 3 [38], and 4 [38,39]). Similar proton affinities between alcohol and alkanal (e.g., 786.5 kJ mol^{-1} and 786 kJ mol^{-1} for n -propanol and propanal, respectively [40]) suggest that the proton transfer step may also occur readily in alkanals, thus species (3), (4a), (4b), and their physisorbed counterparts may interconvert rapidly. Equilibrium between propanal and propenol (Step 2.1a) and between these gas-phase species and their respective adsorbed complexes (Steps 1.1 and 2.2) requires complexes (3), (4a), (4b), and other adsorbed propanal isomers to remain equilibrated with each other within the time-scale of forward propanal turnovers. Rapid interconversion among the various propanal derived surface intermediates renders these species be treated as a kinetically indistinguishable lump, and within this lump, their relative surface abundances are dictated by the differences in their heats of adsorption.

Nucleophilic addition of propenol (2) to the carbonyl group of protonated propanal (3) (Step 1.2) creates an inter-molecular C–C bond and produces a 3-hydroxyl-2-methylpentanal (5). Sequential H_2O elimination (Step 1.3) converts the newly formed C–C bond in the 3-hydroxyl-2-methylpentanal (5) to a C=C bond and increases its degree of unsaturation, and upon desorption (Step 1.4), completes a catalytic turnover to evolve 2-methyl-2-pentenal (7). These mechanistic pathways are analogous to those established in the liquid phase [6,7] and proposed for condensation reactions of acetone on H-MFI samples [41]. The nucleophilic addition step (Step 1.2) is the kinetically-relevant step and this step is reversible, as shown in Section 3.5. Quasi-equilibrium assumptions for Steps 1.1, 1.3, 1.4, 2.1a, 2.1b, 2.2, 2.4, and 2.5 in Scheme 2, together with pseudo steady-state approximation on all reactive intermediates, lead to the following rate expression for inter-molecular C=C bond formation (r_{inter} , per catalytically active H^+ site):

$$r_{\text{inter}} = \frac{k_{\text{aldol}} K_{\text{ads}} K_{\text{taut}} P_{\text{C}_3\text{H}_6\text{O}}^2 - k_{\text{-aldol}} \frac{K_{\text{ads,C}_6\text{H}_{10}\text{O}}}{K_{\text{dehy}}} P_{\text{C}_6\text{H}_{10}\text{O}} P_{\text{H}_2\text{O}}}{1 + K_{\text{ads}} P_{\text{C}_3\text{H}_6\text{O}} + K_{\text{ads}} \sum_{s=1}^n K'_{\text{taut},s} P_{\text{C}_3\text{H}_6\text{O}} + \frac{K_{\text{ads,C}_6\text{H}_{10}\text{O}}}{K_{\text{dehy}}} P_{\text{C}_6\text{H}_{10}\text{O}} P_{\text{H}_2\text{O}} + K_{\text{ads,C}_6\text{H}_{10}\text{O}} P_{\text{C}_6\text{H}_{10}\text{O}} + \frac{K_{\text{ads,C}_3\text{H}_6}}{K_{\text{alkox}}} P_{\text{C}_3\text{H}_6} P_{\text{H}_2\text{O}} + K_{\text{ads,C}_3\text{H}_6} P_{\text{C}_3\text{H}_6}}$$

$$\begin{array}{cccccc} (\text{H}^+) & (\text{C}_3\text{H}_6\text{O}-\text{H}^+) & (\text{C}_3\text{H}_5\text{OH}-\text{H}^+) & (\text{C}_6\text{H}_{12}\text{O}_2-\text{H}^+) & (\text{C}_6\text{H}_{10}\text{O}-\text{H}^+) & (\text{C}_3\text{H}_7\text{OH}-\text{H}^+) & (\text{C}_3\text{H}_7^+-\text{O}) \\ (3) & (4\text{a}), (4\text{b}), \text{ and their} & (5) & (6) & (8) & (9) \\ & \text{physisorbed forms} & & & & & \end{array}$$

where rate and equilibrium constants and the associated catalytic steps are defined in Scheme 2. k_{aldol} and $k_{\text{-aldol}}$ denote the elemen-

tary rate constants for the forward and reverse reactions, respectively, in Step 1.2. K_{ads} , K_{taut} , $K'_{\text{taut},s}$, K_{dehy} , K_{alkox} , $K_{\text{ads,C}_6\text{H}_{10}\text{O}}$, and $K_{\text{ads,C}_3\text{H}_6}$ denote the equilibrium constants for Steps 1.1, 2.1a, 2.1b, 1.3, 2.4, 1.4, and 2.5, respectively. P_x denotes the partial pressure of species x ($x = \text{C}_3\text{H}_6\text{O}$, $\text{C}_6\text{H}_{10}\text{O}$, C_3H_6 , or H_2O). The diverse propanal surface isomers {(4a), (4b), and their physisorbed forms} interconvert rapidly with each other; thus, their overall surface concentration over that of vacant H^+ sites is given by term $K_{\text{ads}} \sum_{s=1}^n K'_{\text{taut},s} P_{\text{C}_3\text{H}_6\text{O}}$ over unity, where $K'_{\text{taut},s}$ is the equilibrium constant for the formation of species s (s represents (4a), (4b), and the physisorbed forms of (4a), (4b), etc.) from protonated propanal (3) (Step 2.1b, Scheme 2), thus term $\sum_{s=1}^n K'_{\text{taut},s}$ represents the aggregated equilibrium constant for the adsorbed propanal isomers. The magnitude of each term in the denominator of Eq. (2) reflects the surface coverage ratio of a specific surface species {(3), (4a), (4b) and their physisorbed forms}, (5), (6), (8), and (9), as labeled in the equation} to unoccupied H^+ sites (the first term in the denominator with a value of unity). The rate expression (Eq. (2)) is simplified to:

$$r_{\text{inter}} = k_{\text{aldol}} \left(\frac{K_{\text{taut}}}{1 + \sum_{s=1}^n K'_{\text{taut},s}} \right) P_{\text{C}_3\text{H}_6\text{O}} = k_{\text{inter,eff}} P_{\text{C}_3\text{H}_6\text{O}} \quad (3)$$

when H^+ sites are occupied by protonated propanal (3), propenol (4a), allyl alcohol (4b), and their physisorbed forms as the most abundant surface intermediates and the reverse rates for the inter-molecular C=C bond formation, which are given by term $k_{\text{-aldol}} K_{\text{ads,C}_6\text{H}_{10}\text{O}} K_{\text{dehy}}^{-1} P_{\text{C}_6\text{H}_{10}\text{O}} P_{\text{H}_2\text{O}}$ in Eq. (2), are insignificant compared with the net rates of this reaction. Eq. (3) accurately describes the first-order dependence measured and presented in Fig. 5, attained under differential conditions and thus at low $\text{C}_6\text{H}_{10}\text{O}$ (7) and H_2O pressures ($P_{\text{C}_6\text{H}_{10}\text{O}} = 0.006\text{--}0.022$ kPa, $P_{\text{H}_2\text{O}} = 0.01\text{--}0.03$ kPa). The effective rate constant in Eq. (1), $k_{\text{inter,eff}}$, equals the proportionality constant $k_{\text{aldol}} \left(K_{\text{taut}} \left(1 + \sum_{s=1}^n K'_{\text{taut},s} \right)^{-1} \right)$ in Eq. (3) and is the product of the forward rate constant for the nucleophilic addition step (k_{aldol} , Step 1.2), equilibrium constants for conversion between propanal and propenol (K_{taut} , Step 2.1a) and between protonated propanal and the various adsorbed propanal isomers ($K'_{\text{taut},s}$, Step 2.1b). Eq. (2) is used to regress against the rate data to extract the kinetic and thermodynamic parameters, to be discussed in Section 3.7.

3.4. Kinetic dependencies, elementary steps, and site requirements for intra-molecular C=C bond formation in propanal on H-MFI zeolites

Next, we provide the rate dependencies and mechanistic evidence for intra-molecular C=C bond formation in propanal by direct removal of oxygen heteroatom while preserving the carbon backbone to evolve propene. The primary nature of this step is

¹ Adsorbed propanal is more stable than allyl alcohol, in their protonated forms, by 71 kJ mol^{-1} , reported in [33] based on the difference in gas-phase proton affinity between these compounds and ammonia and on the heat of ammonia adsorption, assuming similar dispersive interaction energies for these compounds and ammonia with the MFI pore.

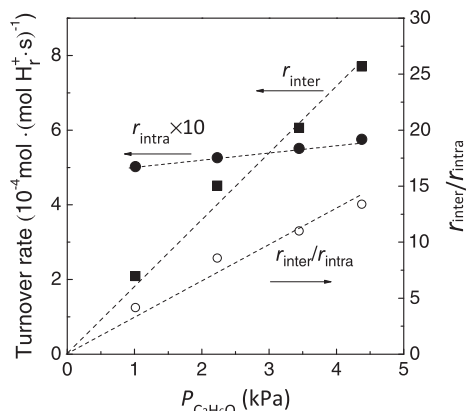


Fig. 5. Turnover rates for inter-molecular C=C bond formation (r_{inter} , ■) and intra-molecular C=C bond formation (r_{intra} , ●) in propanal ($\text{C}_3\text{H}_6\text{O}$) that evolve 2-methyl-2-pentenal ($\text{C}_6\text{H}_{10}\text{O}$) and propylene, respectively, and the rate ratio for inter- over intra-molecular C=C bond formation ($r_{\text{inter}}/r_{\text{intra}}$, ○), plotted as a function of $\text{C}_3\text{H}_6\text{O}$ pressure on H-MFI at 473 K (Si/Al = 11.5, 7.5 ks, 1.1×10^{-3} – 4.4×10^{-3} mol $\text{C}_3\text{H}_6\text{O}$ (mol H^+) $^{-1}$ s $^{-1}$).

confirmed from the near exclusive formation of alkenes (C_nH_{2n} , $n = 3$ –5) from alkanals ($\text{C}_n\text{H}_{2n}\text{O}$, $n = 3$ –5) following the reaction stoichiometry of:



Within the lump of alkene product, the fraction of alkene with carbon number identical to the alkanal reactant from $\text{C}_3\text{H}_6\text{O}$, $\text{C}_4\text{H}_8\text{O}$, and $\text{C}_5\text{H}_{10}\text{O}$ reactions on H-MFI zeolites, i.e. $[\text{C}_3\text{H}_6]/[\text{C}_n\text{H}_{2n}]$, $[\text{C}_4\text{H}_8]/[\text{C}_n\text{H}_{2n}]$, and $[\text{C}_5\text{H}_{10}]/[\text{C}_n\text{H}_{2n}]$, are 0.93, 0.95, and 0.89, respectively, at 473 K and high space velocity $\{1.1 \times 10^{-3}$ mol $\text{C}_n\text{H}_{2n}\text{O}$ (mol H^+) $^{-1}$ s $^{-1}$ } at which sequential conversions of alkene remain negligible [42].

Turnover rates for intra-molecular C=C bond formation (r_{intra}) during propanal reactions on H-MFI (Si/Al = 11.5) at 473 K are essentially insensitive to propanal pressure (1.1–4.5 kPa), as shown in Fig. 5, and equal to the effective rate constant $k_{\text{intra,eff}}$:

$$r_{\text{intra}} = k_{\text{intra,eff}} P_{\text{C}_3\text{H}_6\text{O}}^0 \quad (5)$$

This rate dependence is consistent with the proposed mechanism in Scheme 2. Propanal molecules first encounter H^+ sites and adsorb as protonated species (3), which interconvert to diverse isomeric surface species ((4a), (4b), and their physisorbed isomers), as described in Section 3.3. As these isomeric species interconvert, a portion of them accepts hydrogen from hydrogen-donating agents (identity and origin to be discussed in Section 3.6) in a kinetically-relevant hydrogen transfer step (Step 2.3) to increase their degree of saturation and form adsorbed propanol (8). The adsorbed propanol undergoes sequential dehydration (Step 2.4) to form surface propoxide (9) [43–46] before desorption as propene (10) (Step 2.5). The dehydration step occurs after the hydrogen transfer step and remains kinetically inconsequential (to be confirmed in Section 3.6). These assumptions, together with pseudo steady-state approxima-

tion applied to the various surface intermediates in Scheme 2, give the following rate expression for intra-molecular C=C bond formation (r_{intra} , per catalytically active H^+ site):

The elementary rate and equilibrium constants in Eq. (6) are defined in the previous section and provided in Scheme 2. $k_{\text{H trans}}$ represents the effective rate constant for hydrogen transfer (Step 2.3) and $P_{\text{R}'\text{H}_2}$ denotes the aggregate partial pressure of hydrogen donors, defined here as a pool of species formed from secondary reactions (R 1.3.1 and 1.3.2, Scheme 1) that donate hydrogen atoms (Step 2.3) to increase their extent of unsaturation. The kinetic relevance of hydrogen transfer (Step 2.3), kinetic irrelevance of propanal dehydration step (Step 2.4), and identity of hydrogen donors are probed and confirmed in Section 3.6. The term $k_{\text{H trans}} P_{\text{R}'\text{H}_2}$ in Eq. (6) is defined as:

$$k_{\text{H trans}} P_{\text{R}'\text{H}_2} = \sum_{j=1}^m k_{\text{H trans},j} P_{\text{R}'\text{H}_2,j} \quad (7)$$

where $P_{\text{R}'\text{H}_2,j}$ and $k_{\text{H trans},j}$ are the pressure and hydrogen transfer rate constant for each specific hydrogen donor j (e.g., 6,8-dimethyl-1,2,3,4-tetrahydronaphthalene, Scheme 1), formed from secondary ring closure reactions (R 1.3.1, Scheme 1). The rates for intra-molecular C=C bond formation (Fig. 5) were measured at similar conversions (1.2–1.5%) while individual pressures of hydrogen donors were maintained at similar values (the total pressure of aromatics varied from 4.5×10^{-4} to 6.5×10^{-4} kPa), thus $k_{\text{H trans}} P_{\text{R}'\text{H}_2}$ in Eq. (6) is treated as a constant value in our kinetic analysis (Section 3.7). Turnover rates for intra-molecular C=C bond formation (r_{intra} , Eq. (6)) become independent of propanal pressure and their values equal the effective rate constant for intra-molecular C=C bond formation ($k_{\text{intra,eff}}$), when H^+ sites are predominantly occupied by protonated propanal (3) and its isomers ((4a), (4b), and their physisorbed forms) during steady-state catalysis:

$$r_{\text{intra}} = \left(\frac{\sum_{s=1}^n K'_{\text{taut},s}}{1 + \sum_{s=1}^n K'_{\text{taut},s}} \right) k_{\text{H trans}} P_{\text{R}'\text{H}_2} P_{\text{C}_3\text{H}_6\text{O}}^0 = k_{\text{intra,eff}} P_{\text{C}_3\text{H}_6\text{O}}^0 \quad (8)$$

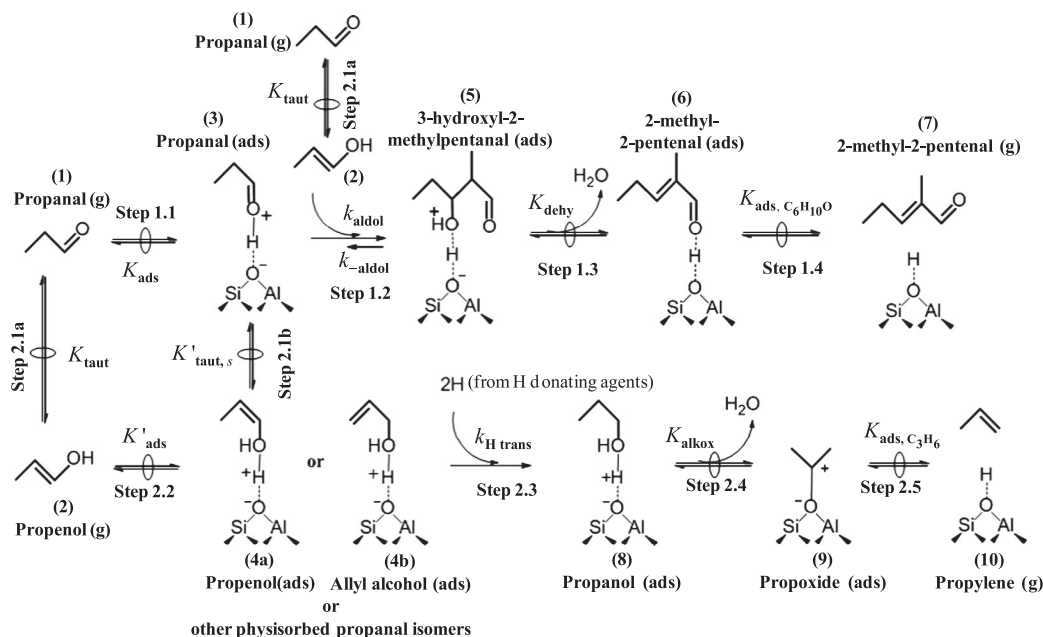
Eq. (8) describes the measured rates for intra-molecular C=C bond formation in Fig. 5, which remain largely insensitive to propanal pressure (with an apparent reaction order with respect to $\text{C}_3\text{H}_6\text{O}$ of 0.09 ± 0.02). The slight increase in rates with propanal pressure reflects the increase in hydrogen transfer probabilities as the pressures of hydrogen donors ($P_{\text{R}'\text{H}_2}$, limited to a portion of the aromatic species produced, see Section 3.6) increase slightly with increasing propanal pressure (a 4-fold increase in $\text{C}_3\text{H}_6\text{O}$ pressure leads to ~50% variation in the partial pressure of total aromatics during rate measurements).

3.5. Reversibility of the inter- and intra-molecular C=C bond formation in propanal on H-MFI zeolites

The influence of H_2O on the number of catalytically active sites and on the net rates of inter- and intra-molecular C=C bond formation was probed by propanal reactions in excess H_2O (5–10 kPa H_2O , $\text{H}_2\text{O}/\text{C}_3\text{H}_6\text{O} = 4.5$ –9). Pyridine titration carried out after stea-

$$r_{\text{intra}} = \frac{K_{\text{ads}} \sum_{s=1}^n K'_{\text{taut},s} k_{\text{H trans}} P_{\text{R}'\text{H}_2} P_{\text{C}_3\text{H}_6\text{O}}}{1 + K_{\text{ads}} P_{\text{C}_3\text{H}_6\text{O}} + K_{\text{ads}} \sum_{s=1}^n K'_{\text{taut},s} P_{\text{C}_3\text{H}_6\text{O}} + \frac{K_{\text{ads},\text{C}_6\text{H}_{10}\text{O}}}{K_{\text{dehy}}} P_{\text{C}_6\text{H}_{10}\text{O}} P_{\text{H}_2\text{O}} + K_{\text{ads},\text{C}_6\text{H}_{10}\text{O}} P_{\text{C}_6\text{H}_{10}\text{O}} + \frac{K_{\text{ads},\text{C}_3\text{H}_6}}{K_{\text{alkox}}} P_{\text{C}_3\text{H}_6} P_{\text{H}_2\text{O}} + K_{\text{ads},\text{C}_3\text{H}_6} P_{\text{C}_3\text{H}_6}} \quad (6)$$

$$\begin{array}{ccccccc} (\text{H}^+) & (\text{C}_3\text{H}_6\text{O}-\text{H}^+) & (\text{C}_3\text{H}_5\text{OH}-\text{H}^+) & (\text{C}_6\text{H}_{12}\text{O}_2-\text{H}^+) & (\text{C}_6\text{H}_{10}\text{O}-\text{H}^+) & (\text{C}_3\text{H}_7\text{OH}-\text{H}^+) & (\text{C}_3\text{H}_7^+-\text{O}) \\ (3) & (4a), (4b), \text{ and their} & (5) & (6) & (8) & (9) & \\ & \text{physisorbed forms} & & & & & \end{array}$$



Scheme 2. Mechanism for inter- and intra-molecular C=C bond formation in propanal (C_3H_6O) evolving 2-methyl-2-pentenal ($C_6H_{10}O$) and propylene, respectively, on H^+ sites (\rightleftharpoons denotes quasi equilibrated step, \rightleftharpoons reversible step, and \longrightarrow irreversible step). In $K'_{\text{taut},s}$ of Step 2.1b, species s denotes propanal surface isomers ((4a), (4b), and their physisorbed isomers).

dy-state reactions with $C_3H_6O-H_2O$ mixtures was used to determine the number of active sites that were free of larger, inactive carbonaceous species and thus participated in catalytic turnovers. Table 1 summarizes the pyridine uptakes measured after steady-state reactions in $C_3H_6O-H_2O$ mixtures {7.5 ks, 473 K, 0.01–9 H_2O/C_3H_6O ratios, 1.1×10^{-3} mol C_3H_6O (mol H^+) $^{-1}$ }. Pyridine uptakes were higher when introducing H_2O together with C_3H_6O reactant; their values paralleled the increase in H_2O/C_3H_6O ratio, because H_2O scavenges the carbonaceous species, prevents site occupation, and thus retards catalyst deactivation. Similar effects of H_2O were found during methanol-to-olefins reactions on similar catalysts (H-MFI [47–49]) and SAPO-34 [50,51] at higher temperatures (573–723 K).

Turnover rates for inter- and intra-molecular C=C bond formation in $C_3H_6O-H_2O$ mixtures are plotted against the H_2O pressure in Fig. 6. The rates for inter-molecular C=C bond formation decreased from 2.2×10^{-4} mol (mol H^+) $^{-1}$ s $^{-1}$ to 1.5×10^{-4} mol (mol H^+) $^{-1}$ s $^{-1}$ (the subscript “r” represents H^+ sites available for propanal turnovers, determined from pyridine titration, Section 2.3) as the H_2O pressure increased from ~ 0.011 to 10 kPa. These effects of H_2O reflect an increase in the reverse rate of the nucleophilic addition step (Step 1.2, Scheme 2) at high H_2O pressures, as the numerator term [$k_{\text{-aldol}}K_{\text{ads},C_6H_{10}O}(K_{\text{dehy}})^{-1}P_{C_6H_{10}O}P_{H_2O}$] of Eq. (2) increases to a magnitude comparable to term $k_{\text{aldol}}K_{\text{ads}}K_{\text{taut}}P_{C_3H_6O}^2$ of the same equation. As a result, the net rate

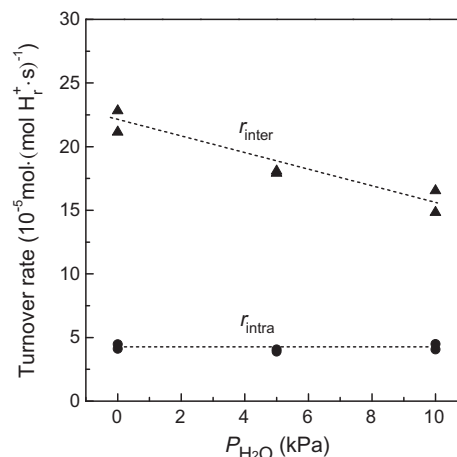


Fig. 6. Effects of water on turnover rates for intra-molecular C=C bond formation (r_{intra} , ●) and inter-molecular C=C bond formation (r_{inter} , ▲) in propanal (C_3H_6O) during C_3H_6O reactions on H-MFI at 473 K (Si/Al = 11.5, 7.5 ks, 1.1×10^{-3} mol C_3H_6O (mol H^+) $^{-1}$, 1.1 kPa C_3H_6O in He).

for inter-molecular C=C bond formation in Eq. (2) decreases and acquires the form of:

$$r_{\text{inter}} = k_{\text{aldol}} \left(\frac{K_{\text{taut}}}{1 + \sum_{s=1}^n K'_{\text{taut},s}} \right) P_{C_3H_6O} - k_{\text{-aldol}} \left(\frac{K_{\text{ads},C_6H_{10}O} K_{\text{dehy}}^{-1}}{K_{\text{ads}} \left(1 + \sum_{s=1}^n K'_{\text{taut},s} \right)} \right) \frac{P_{C_6H_{10}O} P_{H_2O}}{P_{C_3H_6O}} = k_{\text{inter,eff}} P_{C_3H_6O} - k_{\text{-inter,eff}} \frac{P_{C_6H_{10}O} P_{H_2O}}{P_{C_3H_6O}} \quad (9)$$

In contrast, the rates of intra-molecular C=C bond formation did not vary at detectable extents and maintained at $4.2 \times 10^{-5} \pm 0.1 \times 10^{-5}$ mol (mol H^+) $^{-1}$ s $^{-1}$ (Fig. 6). The lack of H_2O effects indicates that H_2O as a by-product does not alter the net rate of intra-molecular C=C bond formation, thus the kinetically-relevant hydrogen transfer step is irreversible. The lack of H_2O effects was also found during

Table 1
Pyridine uptakes on H-MFI zeolites from pyridine titration carried out after steady-state reactions in $C_3H_6O-H_2O$ mixtures^a.

H_2O pressure (kPa)	H_2O/C_3H_6O ratio	Pyridine uptake (10^{-6} mol g_{cat}^{-1})	Pyridine/ H^+ ratio
~ 0.011	~ 0.01	40	0.036
5	4.5	60	0.054
10	9	59	0.053

^a Si/Al = 11.5, 473 K, 7.5 ks, 1.1 kPa C_3H_6O , 0.011–10 kPa of H_2O , space velocity = 1.1×10^{-3} mol C_3H_6O (mol H^+) $^{-1}$ s $^{-1}$. H^+ denotes the number of Brønsted acid sites present initially (measured from pyridine titration after treating the H-MFI samples under flowing He).

allyl alcohol (a propanal isomer) conversion to olefins (predominantly C₃H₆) on NaHY zeolites at 523 K [52], which may occur via similar mechanistic steps. The lack of H₂O effects on the intra-molecular C=C bond formation also precludes the mechanistic sequence involving reversible H₂O elimination from propenol to evolve surface allylic alkoxides before hydrogen insertion, because this case would lead the rates for intra-molecular C=C bond formation to decrease with increasing H₂O pressure. The rate of olefin formation from dehydration of alcohol on Brønsted acid catalysts (e.g., *n*-butanol on H-MFI [53], *sec*-butyl alcohol on H-MFI [54], and 2-propanol on H-MOR [55]) was found to be zero-order at low alcohol pressures (0.6–2 kPa). The zero-order rate constant for *n*-butanol dehydration on H-MFI was estimated to be $2 \times 10^{-2} \text{ mol} (\text{mol H}^+ \text{ s})^{-1}$ at 473 K, determined from extrapolation using the Arrhenius relation from 378 to 458 K [53]. Dehydration of 1-propanol at conditions similar to the propanal rate measurements reported here (0.55 kPa 1-propanol, $6 \times 10^{-4} \text{ mol 1-propanol} (\text{mol H}^+ \text{ s})^{-1}$, 473 K) led to complete conversion to propene and to a zero-order rate constant larger than $1.5 \times 10^{-2} \text{ mol} (\text{mol H}^+ \text{ s})^{-1}$ at 473 K. Taken together the rate constant values for 1-propanol and *n*-butanol dehydration at comparable conditions, we conclude that 1-propanol dehydration rate must be at least two orders of magnitude larger than the direct propanal deoxygenation rate to propene $\{1.5 \times 10^{-4} - 2.2 \times 10^{-4} \text{ mol} (\text{mol H}^+ \text{ s})^{-1}\}$ at 473 K, thus the H₂O elimination step cannot be the kinetically-relevant step for the intra-molecular C=C bond formation in propanal.

These results led us to conclude that catalytic roles of H₂O involve protecting the active sites from occupation by larger, inactive species and altering the net rates for inter-molecular C=C bond formation by promoting the reverse reaction. H₂O, however, does not alter the net rates for intra-molecular C=C bond formation because of its irreversible nature. Next, we probe the kinetic relevance of hydrogen transfer for intra-molecular C=C bond formation in propanal, the kinetic coupling of this step to the secondary dehydrogenation reactions, and identify the hydrogen transfer agents participated in the dehydrogenation steps within the reaction network.

3.6. Kinetic relevance of hydrogen transfer and requirements of hydrogen for intra-molecular C=C bond formation in propanal

The direct deoxygenation route (Eq. (4)) for intra-molecular C=C bond formation in propanal requires oxygen removal from propanal by combining the oxygen heteroatom with two external hydrogen atoms (R 2.2 in Scheme 1 and Step 2.3 in Scheme 2) to eject H₂O. The rate ratios for the overall CO and CO₂ formation to propene formation were lower than 0.1 at 473 K $\{(r_{\text{CO}} + r_{\text{CO}_2})/r_{\text{overall}}\} < 0.01$, thus the oxygen in propanal does not eject as CO or CO₂ but instead as H₂O, as also confirmed from the near exclusive formation of propene $([\text{C}_3\text{H}_6]/[\text{C}_n\text{H}_{2n}]) = 0.93$, 473 K) within the alkene fractions (Section 3.4).

A detailed structural analysis of the diverse aromatic and olefinic species in the effluent stream led us to propose that a portion of hydronaphthalenes (e.g., 6,8-dimethyl-1,2,3,4-tetrahydronaphthalene) with 10–15 carbons are the hydrogen donors via dehydrogenation steps that increase their aromaticity (R 1.3.2 and 1.3.3, Scheme 1). The amount of H made available from the dehydrogenation steps was determined to be $9.7 \times 10^{-6} \text{ mol H} (\text{g}_{\text{cat}} \text{ s})^{-1}$ at 673 K {reaction conditions of 1.1 kPa C₃H₆O and $1.1 \times 10^{-3} \text{ mol C}_3\text{H}_6\text{O} (\text{mol H}^+ \text{ s})^{-1}$ }, quantified here based on the amount of aromatics (dihydronaphthalenes and naphthalenes) formed (Fig. 2d) as a result of H donation (reactions R 1.3.2 and 1.3.3, Scheme 1) during steady-state catalysis. This amount is consistent with the hydrogen amount required for the formation of diverse olefinic species (R 2.2 and R 3, Scheme 1), calculated to be $9.0 \times 10^{-6} \text{ mol H} (\text{g}_{\text{cat}} \text{ s})^{-1}$, based on the alkene distributions in

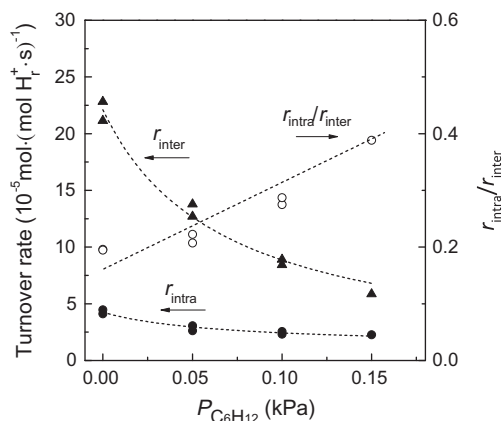


Fig. 7. Effects of 3-methyl-1-pentene (C₆H₁₂) pressure on intra-molecular C=C bond formation (r_{intra} , ●) and inter-molecular C=C bond formation (r_{inter} , ▲) in propanal (C₃H₆O) and the rate ratio for intra- over inter-molecular C=C bond formation ($r_{\text{inter}}/r_{\text{intra}}$, ○) during C₃H₆O reactions on H-MFI catalysts at 473 K (Si/Al = 11.5, 7.5 ks, $1.1 \times 10^{-3} \text{ mol C}_3\text{H}_6\text{O} (\text{mol H}^+ \text{ s})^{-1}$, 1.1 kPa C₃H₆O in He).

the product of the same reaction (Fig. 2d, 673 K). These results indicate that intra-molecular C=C bond formation requires H transfer to satisfy the reaction stoichiometry, and in the absence of an external hydrogen source, the hydrogen must come from secondary dehydrogenation events. The kinetic coupling of intra-molecular C=C bond formation and dehydrogenation steps thus dictates the distributions of olefinic and aromatic species formed from propanal reactions.

The kinetic relevance of the hydrogen transfer step was probed by measuring rates in the presence of 3-methyl-1-pentene (CH₂=CH₂CH(CH₃)C₂H₅, denoted hereinafter as C₆H₁₂) as an effective hydrogen donor [56], because of its weak tertiary allylic C–H bond (323 kJ mol⁻¹ [57]). Fig. 7 shows the effects of C₆H₁₂ pressure on the turnover rates for inter- and intra-molecular C=C bond formation (r_{inter} and r_{intra} , respectively) in C₃H₆O–C₆H₁₂ mixtures on H-MFI at 473 K.

Both the turnover rates for inter- and intra-molecular C=C bond formation decreased as C₆H₁₂ pressure increased, because C₆H₁₂ species titrated a portion of the adsorbed propanal (and its isomers), as expected from the higher proton affinity ($\sim 813 \text{ kJ mol}^{-1}$ for C₆H₁₂² vs. 786 kJ mol⁻¹ for C₃H₆O [40]) and higher dispersive interactions as they adsorb on MFI zeolites (increased by 15 kJ mol⁻¹ for each additional C atom in alcohol [38,58] and 10–12 kJ mol⁻¹ for each additional C atom in alkane [27,59,60]) for C₆H₁₂ than C₃H₆O. The rates for intra-molecular C=C bond formation (r_{intra}), however, decreased to a much lower extent than those for inter-molecular C=C bond formation, because C₆H₁₂ promotes the kinetically-relevant hydrogen transfer step (Step 2.3, Scheme 2) but does not affect the nucleophilic addition step (Step 1.2, Scheme 2).

The rates of inter-molecular C=C bond formation in C₃H₆O–C₆H₁₂ mixtures ($r_{\text{inter,C}_3\text{H}_6\text{O-C}_6\text{H}_{12}}$) acquire an additional dependence on C₆H₁₂ pressure; thus Eq. (2) becomes:

$$r_{\text{inter,C}_3\text{H}_6\text{O-C}_6\text{H}_{12}} = \frac{k_{\text{aldol}} K_{\text{ads}} K_{\text{taut}} P_{\text{C}_3\text{H}_6\text{O}}^2}{K_{\text{ads}} P_{\text{C}_3\text{H}_6\text{O}} + K_{\text{ads}} \sum_{s=1}^n K'_{\text{taut},s} P_{\text{C}_3\text{H}_6\text{O}} + K_{\text{ads,C}_6\text{H}_{12}} P_{\text{C}_6\text{H}_{12}}}$$

$$\begin{matrix} (\text{C}_3\text{H}_6\text{O-H}^+) & (\text{C}_3\text{H}_5\text{OH-H}^+) & (\text{C}_6\text{H}_{12}\text{-H}^+) \\ \text{(3)} & \text{(4a), (4b), and their} & \\ & \text{physisorbed forms} & \end{matrix} \quad (10)$$

² Proton affinity of 3-methyl-1-pentene is estimated from other C₆H₁₂ molecules with closely related structure: 2-methyl-2-pentene (812 kJ mol⁻¹) and 2,3-dimethylbutene (813.9 kJ mol⁻¹).

when H⁺ sites are predominantly occupied by protonated propanal and its isomers (**(3)**, **(4a)**, **(4b)**, and their physisorbed forms} and C₆H₁₂ as the most abundant surface intermediates. $P_{C_6H_{12}}$ and $K_{ads,C_6H_{12}}$ denote the partial pressure of C₆H₁₂ and the equilibrium constant for C₆H₁₂ adsorption on H⁺ sites, respectively.

The rates of intra-molecular C=C bond formation ($r_{intra,C_3H_6O-C_6H_{12}}$) contain two distinct rate constants for hydrogen transfer reactions with a portion of aromatics (predominantly hydronaphthalenes) ($k_{H\ trans}$) and C₆H₁₂ ($k_{H\ trans,C_6H_{12}}$) as the H donating agents, because C₆H₁₂ and hydronaphthalenes both participate as hydrogen donors but at different rates as a result of the variation in C–H bond strength (e.g., 305–315 kJ mol⁻¹ and 319–323 kJ mol⁻¹ for the α-H of hydronaphthalene and C₆H₁₂, respectively [57]):

$$r_{intra,C_3H_6O-C_6H_{12}} = \frac{(k_{H\ trans}P_{R'H_2} + k_{H\ trans,C_6H_{12}}P_{C_6H_{12}}) \cdot K_{ads} \sum_{s=1}^n K'_{taut,s} P_{C_3H_6O}}{K_{ads} \left(1 + \sum_{s=1}^n K'_{taut,s}\right) P_{C_3H_6O} + K_{ads,C_6H_{12}} P_{C_6H_{12}}} \quad (11)$$

The term $k_{H\ trans}P_{R'H_2}$ corresponds to the rate of hydrogen donation from aromatics, as defined in Eq. (7), and the rest of the kinetic and thermodynamic parameters are defined in Sections 3.3 (Eq. (2)), 3.4 (Eqs. (6) and (7)), and 3.6 (Eq. (10)). The total pressure of aromatics varied from 4.5×10^{-4} to 7.0×10^{-4} kPa during propanal catalysis in C₃H₆O (without C₆H₁₂) (1.1–4.5 kPa C₃H₆O, Fig. 5) and in C₃H₆O–C₆H₁₂ mixtures (0–0.15 kPa C₆H₁₂, 1.1 kPa C₃H₆O, Fig. 7). As a result, pressures of the portion of aromatics that act as hydrogen donors ($P_{R'H_2}$) must also remain at similar values despite the changes in C₆H₁₂ and C₃H₆O pressures during rate measurements. Therefore, term $k_{H\ trans}P_{R'H_2}$ in Eq. (11) is approximated as a constant. Combining Eqs. (11) and (10), the rate ratio for intra-molecular to inter-molecular C=C bond formation (r_{intra}/r_{inter}) is given by:

$$\frac{r_{intra}}{r_{inter}} = \frac{\sum_{s=1}^n K'_{taut,s} (k_{H\ trans}P_{R'H_2} + k_{H\ trans,C_6H_{12}}P_{C_6H_{12}})}{k_{aldol}K_{taut}P_{C_3H_6O}} \quad (12)$$

This expression predicts a linear increase in r_{intra}/r_{inter} with C₆H₁₂ pressure when the pressures of propanal ($P_{C_3H_6O}$) and hydrogen donors ($P_{R'H_2}$, e.g., 6,8-dimethyl-1,2,3,4-tetrahydronaphthalene, Scheme 1) were held relatively constant as the C₆H₁₂/C₃H₆O ratio was varied from 0 to 0.15, as is shown in Fig. 7. The selective promotion of C₆H₁₂ towards the hydrogen transfer step over the nucleophilic addition step partially compensates for the reduction in propanal surface coverage and leads, in turn, to an increase in the rate ratio for intra-molecular over inter-molecular C=C bond formation, r_{intra}/r_{inter} , with increasing C₆H₁₂ pressure.

Table 2

Rate parameters derived from non-linear regression fittings of rate data to rate equations (Eqs. (8), (9), (A.2), and (A.3) (in Appendix A)).

Parameter	Value
$k_{inter,eff} = k_{aldol} \left(\frac{K_{taut}}{1 + \sum_{s=1}^n K'_{taut,s}} \right)^a$	$1.97 \times 10^{-4} \pm 0.06 \times 10^{-4} \text{ s}^{-1} \text{ kPa}^{-1}$
$k_{-inter,eff} = k_{-aldol} \left(\frac{K_{ads,C_6H_{10}O}}{K_{dehy}K_{ads} \left(1 + \sum_{s=1}^n K'_{taut,s} \right)} \right)^a$	$9.5 \times 10^{-4} \pm 1.8 \times 10^{-4} \text{ s}^{-1} \text{ kPa}^{-1}$
$k_{intra,eff} = \left(\frac{\sum_{s=1}^n K'_{taut,s}}{1 + \sum_{s=1}^n K'_{taut,s}} \right) k_{H\ trans} P_{R'H_2}^b$	$4.18 \times 10^{-5} \pm 0.10 \times 10^{-5} \text{ s}^{-1}$
$\frac{K_{ads,C_6H_{12}}}{\left(1 + \sum_{s=1}^n K'_{taut,s} \right) K_{ads}}^c$	15.9 ± 1.2
$\frac{k_{H\ trans,C_6H_{12}}}{k_{H\ trans} P_{R'H_2}}^c$	$4.3 \pm 0.6 \text{ kPa}^{-1}$

^a Estimated values for kinetic parameters in Eq. (9); see Appendix A for the determination of $k_{inter,eff}$ and $k_{-inter,eff}$.

^b Estimated values for kinetic parameters in Eq. (8).

^c Estimated values for kinetic parameters in Eqs. (A.2) and (A.3) (in Appendix A).

3.7. Regression of rate data with the derived rate expressions for inter- and intra-molecular C=C bond formation

Rate equations derived for inter- and intra-molecular C=C bond formation from Sections 3.3–3.6 (Eqs. (8)–(11)) were used to regress against the rate data from C₃H₆O, C₃H₆O–H₂O, and C₃H₆O–C₆H₁₂ reactions over H-MFI at 473 K, presented in Figs. 5–7, and (A.3) (in Appendix A), to obtain the estimated kinetic and thermodynamic parameters in Table 2.

The effective rate constant for inter-molecular C=C bond formation ($k_{inter,eff}$) is:

$$k_{inter,eff} = k_{aldol} \left(\frac{K_{taut}}{1 + \sum_{s=1}^n K'_{taut,s}} \right) \approx k_{aldol} K_{taut} \quad \text{for } 1 \gg \sum_{s=1}^n K'_{taut,s} \quad (13)$$

and its value was found to be $1.97 \times 10^{-4} \pm 0.06 \times 10^{-4} \text{ s}^{-1} \text{ kPa}^{-1}$ at 473 K. The two terms in the denominator of Eq. (13), 1 and $\sum_{s=1}^n K'_{taut,s}$, correspond to the coverages of the protonated propanal (**(3)**, Scheme 2) and adsorbed propanal isomers {propanol (**(4a)**), allyl alcohol (**(4b)**, and their physisorbed forms}, respectively. Protonated propanal (**(4a)**) and allyl alcohol (**(4b)**) were estimated to be 94 kJ mol⁻¹ and 71 kJ mol⁻¹ less stable than protonated propanal (**(3)**) in H-MFI zeolites, based on their relative proton affinities with ammonia and on the heat of ammonia adsorption but not accounting for the difference in dispersive interaction energies between these species and the MFI pore walls [33]. Similar trends and values are expected for the physisorbed species because of the small energy differences between the protonated and physisorbed species [36–39]. The relative magnitudes of these heats of adsorption suggest that the second term $\sum_{s=1}^n K'_{taut,s}$ is much smaller than 1, thus $k_{inter,eff}$ is approximated to be equal to $k_{aldol}K_{taut}$.

The rate constant for the reverse reaction (reverse of Step 1.2, Scheme 2), $k_{-inter,eff}$, for inter-molecular C=C bond formation was found to be $9.5 \times 10^{-4} \pm 1.8 \times 10^{-6} \text{ s}^{-1} \text{ kPa}^{-1}$, a magnitude similar to the forward rate constant ($1.97 \times 10^{-4} \pm 0.06 \times 10^{-4} \text{ s}^{-1} \text{ kPa}^{-1}$) at 473 K. This reaction becomes reversible as the conversion increases and in the limit of high $P_{H_2O}/P_{C_3H_6O}$ (e.g., $r_{reverse,inter}/r_{net,inter} = 0.45$ when $P_{H_2O}/P_{C_3H_6O} = 9$, 473 K) or high $P_{C_6H_{10}O}/P_{C_3H_6O}$ (not shown here) ratios. The reverse rates are unimportant and do not affect the net rates at the low C₆H₁₀O and H₂O pressures used in the rate measurements for obtaining the rate data reported in Fig. 6 ($P_{C_6H_{10}O}/P_{C_3H_6O} = 0.005–0.01$). Turnover rates for the intra-molecular C=C bond formation equal the effective rate constant $k_{intra,eff}$ (Eq. (8)) and depend on the aggregate values of the elementary rate constants for hydrogen transfer ($k_{H\ trans}$) and the pressures of hydrogen donors ($P_{R'H_2}$), as defined in Eq. (7), and the sum of equilibrium constants for propanal adsorption at various conformations ($\sum_{s=1}^n K'_{taut,s}$, as defined in Section 3.3, Eq. (2)). These effects of pressures and rate constants were lumped and treated here as a pseudo rate constant, because the pressures of the hydrogen donors were relatively constant during rate measurements (Section 3.6):

$$k_{intra,eff} = \left(\frac{\sum_{s=1}^n K'_{taut,s}}{1 + \sum_{s=1}^n K'_{taut,s}} \right) k_{H\ trans} P_{R'H_2} \quad (14)$$

These assumptions (Eqs. (13) and (14)), upon substitution into Eq. (12), give the rate ratio for inter-molecular over intra-molecular C=C bond formation, which reflects the selectivity ratio for C₆H₁₀O (2-methyl-2-pentenal) to C₃H₆ formation in the primary reaction paths ($S_{C_6H_{10}O/C_3H_6}$):

$$S_{C_6H_{10}O/C_3H_6} = \frac{r_{inter}}{r_{intra}} = \frac{k_{aldol}K_{taut}P_{C_3H_6O}}{\sum_{s=1}^n K'_{taut,s} (k_{H\ trans}P_{R'H_2} + k_{H\ trans,C_6H_{12}}P_{C_6H_{12}})} \quad (15)$$

The selectivities towards $C_6H_{10}O$, according to Eq. (15), are expected to increase with increasing propanal pressure (Fig. 5), because higher propanal pressure favors the inter-molecular over intra-molecular C=C bond formation.

Non-linear regression of the rate data measured in C_3H_6O – C_6H_{12} mixtures (Fig. 7) against Eqs. (A.2) and (A.3) (rearranged in simplified forms from Eqs. (10) and (11), respectively, see Appendix A) gives the rate parameters for hydrogen transfer (Table 2). The term $k_{H\text{ trans}, C_6H_{12}} (k_{H\text{ trans}} P_{R'H_2})^{-1}$ (from Eq. (A.3)) represents the relative reactivities of C_6H_{12} to hydronaphthalene species as hydrogen donors; its value was found to be $4.3 \pm 0.8 \text{ kPa}^{-1}$ (473 K). The rate data reported in Fig. 7 were measured at aromatic pressures of less than 10^{-3} kPa , and within the aromatic lump only a small portion of them acting as hydrogen donors. Substituting 10^{-3} kPa as the maximum value of hydrogen donor pressure (as $P_{R'H_2}$) gives $k_{H\text{ trans}, C_6H_{12}} (k_{H\text{ trans}})^{-1}$ ratio of 4.3×10^{-3} . The $k_{H\text{ trans}, C_6H_{12}} (k_{H\text{ trans}})^{-1}$ ratio much lower than unity is consistent with much lower reactivities for hydrogen transfer in C_6H_{12} than in hydronaphthalene species, as predicted from the differences in their C–H bond strength (estimated to be 319–323 kJ mol^{-1} for the tertiary allylic C–H bond in C_6H_{12} [57] vs. 305–315 kJ mol^{-1} for the H leaving group in hydronaphthalene [57]). The ratio $K_{\text{ads}, C_6H_{12}} \left[\left(1 + \sum_{s=1}^n K'_{\text{taut},s} \right) K_{\text{ads}} \right]^{-1}$ were estimated to be 16.5 ± 1.7 , a value larger than unity and indicates a higher heat of adsorption for C_6H_{12} than those for propanal and its isomers ((3), (4a), (4b) and their physisorbed forms, Scheme 2) on H-MFI zeolite, consistent with the trend in their proton affinity and dispersive interaction energy (Section 3.6). These studies highlight the key requirements that determine the catalytic fate of propanal to either lengthen or preserve its carbon chain length during its catalytic sojourns on H^+ sites. These mechanistic insights would allow us to quantitatively predict and control rates and product distributions.

4. Conclusion

Kinetic interrogations and acid site titrations lead to a proposed sequence of elementary steps for propanal deoxygenation on H^+ sites immobilized within MFI framework. The reaction occurs via competitive pathways of inter- and intra-molecular C=C bond formation that evolve 2-methyl-2-pentenal and propene, respectively. The inter-molecular C=C form formation occurs via coupling of propanal and intra-molecular C=C bond formation via direct oxygen removal as H_2O . These reactions proceed in parallel with distinct rate dependencies on Brønsted acid sites predominantly occupied by protonated propanal and its isomers, which present as a kinetically indistinguishable lump during steady-state catalysis. Rates for inter-molecular propanal coupling increase linearly with propanal pressure and decrease with water pressure and are limited by the nucleophilic attack of propenal to protonated propanal in a bimolecular condensation reaction. The rates of intra-molecular C=C bond formation, however, remain insensitive to propanal pressure, because rates are limited solely by the transfer of hydrogen atom from hydrogen-donating agents to propanal derived surface intermediates. Water as a by-product mitigates site occupation by larger, inactive carbonaceous species and increases the reverse rates for inter-molecular C=C bond formation, thus decreasing the net rates of this step. Water, however, does not affect the net rates for intra-molecular C=C bond formation because this step is irreversible. The kinetic relevance of hydrogen transfer in intra-molecular C=C formation step is confirmed from the increase in the rate ratio for intra- over inter-molecular C=C bond formation as the pressure of hydrogen-donating agent increases. During steady-state catalysis, hydrogen-donating events, enabled by sequential reactions of intra-molecular ring closure and dehydrogenation steps that remove hydrogen and in-

crease the degree of unsaturation in secondary products, and the hydrogen accepting events are kinetically coupled to evolve propene as a primary product. This knowledge on the nature of surface intermediates and kinetic requirements in catalytic rates and selectivities provide the framework on tuning the relative rates for the initial inter- and intra-molecular C=C bond formation in propanal and the product distributions during propanal deoxygenation on Brønsted acid sites contained within the MFI structures.

Acknowledgments

This study was supported by Natural Sciences and Engineering Research Council of Canada and Canada Foundation for Innovation. We thank Yuanshuai Liu and Eszter Barath for their help with the infra-red measurements and technical discussion on acid site quantification.

Appendix A. Supplementary material

Supplementary data associated with this article can be found, in the online version, at <http://dx.doi.org/10.1016/j.jcat.2013.11.018>.

References

- [1] E.I. Gürbüz, E.L. Kunkes, J.A. Dumesic, *Appl. Catal. B* 94 (2010) 134–141.
- [2] G.W. Huber, S. Iborra, A. Corma, *Chem. Rev.* 106 (2006) 4044–4098.
- [3] A.G. Gayubo, A.T. Aguayo, A. Atutxa, R. Aguado, M. Olazar, J. Bilbao, *Ind. Eng. Chem. Res.* 43 (2004) 2619–2626.
- [4] T.Q. Hoang, X. Zhu, T. Sooknoi, D.E. Resasco, R.G. Mallinson, *J. Catal.* 271 (2010) 201–208.
- [5] X. Zhu, L.L. Lobban, R.G. Mallinson, D.E. Resasco, *J. Catal.* 271 (2010) 88–98.
- [6] D.S. Kemp, V. Frank, *Organic Chemistry*, Worth Publishers, 1980, pp. 839–845.
- [7] D.S. Noyce, W.A. Pryor, *J. Am. Chem. Soc.* 77 (1955) 1397–1401.
- [8] D.S. Noyce, W.A. Pryor, A.H. Bottini, *J. Am. Chem. Soc.* 77 (1955) 1402–1405.
- [9] A.G. Panov, J.J. Fripiat, *Catal. Lett.* 57 (1999) 25–32.
- [10] T. Komatsu, M. Mitsuhashi, T. Yashima, in: 2nd International Conference of the Federation-of-European-Zeolite-Associations Taormina, Italy, 2002, pp. 667–674.
- [11] A. Ungureanu, S. Royer, T.V. Hoang, D.T. On, E. Dumitriu, S. Kaliaguine, *Micropor. Mesopor. Mater.* 84 (2005) 283–296.
- [12] S.K. Sharma, P.A. Parikh, R.V. Jasra, *J. Mol. Catal. A* 278 (2007) 135–144.
- [13] S.K. Sharma, P.A. Parikh, R.V. Jasra, *Appl. Catal. A* 386 (2010) 34–42.
- [14] W. Shen, G.A. Tompsett, R. Xing, W.C. Conner, G.W. Huber, *J. Catal.* 286 (2012) 248–259.
- [15] R.K. Zeidan, M.E. Davis, *J. Catal.* 247 (2007) 379–382.
- [16] D. Tichit, D. Luitic, B. Coq, R. Durand, R. Teissier, *J. Catal.* 219 (2003) 167–175.
- [17] G.D. Yadav, P. Aduri, *J. Mol. Catal.* 355 (2012) 142–154.
- [18] A. Gangadharan, M. Shen, T. Sooknoi, D.E. Resasco, R.G. Mallinson, *Appl. Catal. A* 385 (2010) 80–91.
- [19] T.Q. Hoang, X. Zhu, L.L. Lobban, D.E. Resasco, R.G. Mallinson, *Catal. Commun.* 11 (2010) 977–981.
- [20] C.D. Chang, A.J. Silvestri, *J. Catal.* 44 (1977) 249–259.
- [21] M. Bjorgen, S. Svelle, F. Joensen, J. Nerlov, S. Kolboe, F. Bonino, L. Palumbo, S. Bordiga, U. Olsbye, *J. Catal.* 249 (2007) 195–207.
- [22] F.J. Keil, *Micropor. Mesopor. Mater.* 29 (1999) 49–66.
- [23] J.F. Haw, W. Song, D.M. Marcus, J.B. Nicholas, *Acc. Chem. Res.* (2003) 317–326.
- [24] A.G. Panov, J.J. Fripiat, *J. Catal.* 178 (1998) 188–197.
- [25] H. Wu, Q. Gong, D.H. Olson, J. Li, *Chem. Rev.* 112 (2012) 836–868.
- [26] J.-R. Li, R.J. Kuppler, H.-C. Zhou, *Chem. Soc. Rev.* 38 (2009) 1477–1504.
- [27] F. Eder, M. Stockenhuber, J.A. Lercher, *J. Phys. Chem. B* 101 (1997) 5414–5419.
- [28] H.v. Bekkum, E.M. Flanigen, P.A. Jacobs, J.C. Jansen, *Introduction to Zeolite Science and Practice*, second ed., Elsevier, 2001.
- [29] Y. Ono, *J. Catal.* 216 (2003) 406–415.
- [30] V.K.D.J. Di Cosimo, C.R. Apesteguia, *Appl. Catal. A* 137 (1996) 149–166.
- [31] M. Xu, W. Wang, M. Hunger, *Chem. Commun.* (2003) 722–723.
- [32] V. Bosacek, L. Kubelkova, *Zeolites* 10 (1990) 64–65.
- [33] A.I. Biaglow, J. Sepa, R.J. Gorte, D. White, *J. Catal.* 154 (1995) 208–215.
- [34] J. Sepa, C. Lee, R.J. Gorte, D. White, *J. Phys. Chem.* 100 (1996) 18515–18523.
- [35] A.I. Biaglow, R.J. Gorte, D. White, *J. Phys. Chem.* 97 (1993) 7135–7137.
- [36] S. Svelle, C. Tuma, X. Rozanska, T. Kerber, J. Sauer, *J. Am. Chem. Soc.* 131 (2009) 816–825.
- [37] F. Haase, J. Sauer, *J. Am. Chem. Soc.* 117 (1995) 3780–3789.
- [38] C.M. Nguyen, M.-F. Reyniers, G.B. Marin, *Phys. Chem. Chem. Phys.* 12 (2010) 9481–9493.
- [39] C.M. Nguyen, M.-F. Reyniers, G.B. Marin, *J. Phys. Chem. C* 115 (2011) 8658–8669.
- [40] E.P.L. Hunter, S.G. Lias, *J. Phys. Chem. Ref. Data* 27 (1998) 413–639.
- [41] A.I. Biaglow, J. Sepa, D.W.R.J. Gorte, *J. Catal.* 151 (1995) 373–384.

- [42] F. Lin, Y.-H. Chin, unpublished results.
- [43] K. Kongpatpanich, T. Nanok, B. Boekfa, M. Probst, J. Limtrakul, *Phys. Chem. Chem. Phys.* 13 (2001) 6462–6470.
- [44] H. Knozinger, *Angew. Chem. Int. Ed.* 7 (1968) 791–805.
- [45] J.N. Kondo, K. Ito, E. Yoda, F. Wakabayashi, K. Domen, *J. Phys. Chem. B* 109 (2005) 10969–10972.
- [46] R.G. Greenler, *J. Chem. Phys.* 37 (1962) 2094–2100.
- [47] A.G. Gayubo, A.T. Aguayo, A.L. Moran, M. Olazar, J. Bilbao, *AIChE J.* 48 (2002) 1561–1571.
- [48] M. Kang, T. Inui, *J. Mol. Catal. A* 140 (1999) 55–63.
- [49] A.G. Gayubo, A. Alonso, B. Valle, A.T. Aguayo, J. Bilbao, *AIChE J.* 58 (2012) 526–536.
- [50] X. Wu, R.G. Anthony, *Appl. Catal. A* 218 (2001) 241–250.
- [51] A.T. Aguayo, A.E.S.d. Campo, A.G. Gayubo, A. Tarrío, J. Bilbao, *J. Chem. Technol. Biot.* 74 (1999) 315–321.
- [52] G.J. Hutchings, D.F. Lee, *Catal. Lett.* 34 (1995) 115–127.
- [53] M.A. Makarova, E.A. Paukshtis, J.M. Thomas, C. Williams, K.I. Zamaraev, *J. Catal.* 149 (1994) 36–51.
- [54] M.A. Makarova, C. Williams, K.I. Zamaraev, J.M. Thomas, *J. Chem. Soc., Faraday Trans. 90* (1994) 2147–2153.
- [55] D.E. Bryant, W.L. Kranich, *J. Catal.* 8 (1967) 8–13.
- [56] D.A. Simonetti, J.H. Ahn, E. Iglesia, *Chem. Catal. Chem.* 3 (2011) 704–718.
- [57] D.F. McMillen, D.M. Golden, *Ann. Rev. Phys. Chem.* 33 (1982) 493–532.
- [58] C.-C. Lee, R.J. Gorte, W.E. Farneth, *J. Phys. Chem. B* 101 (1997) 3811–3817.
- [59] B.A.D. Moor, M.-F. Reyniers, O.C. Gobin, J.A. Lercher, G.B. Marin, *J. Phys. Chem. C* 115 (2011) 1204–1219.
- [60] J.F. Denayer, W. Souverijns, P.A. Jacobs, J.A. Martens, G.V. Baron, *J. Phys. Chem. B* 102 (1998) 4588–4597.